



Identification of promising molecules against MurD ligase from *Acinetobacter baumannii*: insights from comparative protein modelling, virtual screening, molecular dynamics simulations and MM/PBSA analysis

Rajat Kumar Jha¹ · Rameez Jabeer Khan¹ · Gizachew Muluneh Amera¹ · Ekampreet Singh¹ · Amita Pathak² · Monika Jain¹ · Jayaraman Muthukumaran¹ · Amit Kumar Singh¹

Received: 20 May 2020 / Accepted: 21 September 2020 / Published online: 17 October 2020

© Springer-Verlag GmbH Germany, part of Springer Nature 2020

Abstract

Acinetobacter baumannii, an opportunistic bacterium of the multidrug-resistant (MDR) ESKAPE family of pathogens, is responsible for 2–10% infections associated with all gram-negative bacteria. The hospital-acquired nosocomial infections caused by *A. baumannii* include deadly diseases like ventilator-associated pneumonia, bacteremia, septicemia and urinary tract infections (UTI). Over the last 3 years, it has evolved into multiple strains demonstrating high antibiotic resistance against a wide array of antibiotics. Hence, it becomes imperative to identify novel drug-like molecules to treat such infections effectively. UDP-N-acetylmuramoyl-L-alanine-D-glutamate ligase (MurD) is an essential enzyme of the Mur family which is responsible for peptidoglycan biosynthesis, making it a unique and ideal drug target. Initially, a homology modelling approach was employed to predict the three-dimensional model of MurD from *A. baumannii* using MurD from *Escherichia coli* (PDB ID: 4UAG) as a suitable structural template. Subsequently, an optimised model of MurD was subjected to virtual high-throughput screening (vHTS) against a ZINC library of ~642,759 commercially available molecules to identify promising lead compounds demonstrating high binding affinities towards it. From the screening process, four promising molecules were identified based on the estimated binding affinities (ΔG), estimated inhibition constants (K_i), catalytic residue interactions and drug-like properties, which were then subjected to molecular dynamics (MD) simulation studies to reflect the physiological state of protein molecules in vivo equivalently. The binding free energies of the selected MurD-ligand complexes were also calculated using MM/PBSA (molecular mechanics with Poisson-Boltzmann and surface area solvation) approach. Finally, the global dynamics along with binding free energy analysis suggested that ZINC19221101 ($\Delta G = -62.6 \pm 5.6$ kcal/mol) and ZINC12454357 ($\Delta G = -46.1 \pm 2.6$ kcal/mol) could act as most promising candidates for inhibiting the function of MurD ligase and aid in drug discovery and development against *A. baumannii*.

Keywords MurD · *Acinetobacter baumannii* · Molecular docking · MD simulation · ZINC · Structure-based drug design and discovery · MM/PBSA

Rajat Kumar Jha and Rameez Jabeer Khan contributed equally to this work.

Electronic supplementary material The online version of this article (<https://doi.org/10.1007/s00894-020-04557-4>) contains supplementary material, which is available to authorized users.

✉ Amit Kumar Singh
amitk.singh@sharda.ac.in

¹ Department of Biotechnology, School of Engineering and Technology, Sharda University, Greater Noida, U.P. P.C. 201310, India

² Department of Chemistry, Indian Institute of Technology, Hauz Khas, New Delhi 110016, India

Abbreviations

MD	Molecular dynamics simulations
MDRAB	Multidrug-resistant <i>Acinetobacter baumannii</i>
SBDD	Structure-based drug design
vHTS	Virtual high-throughput screening

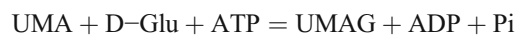
Introduction

Acinetobacter baumannii is an aerobic, non-motile, pleomorphic gram-negative bacterium. It is an opportunistic pathogen in humans, chiefly infecting people with weakened immune

systems [1]. It is responsible for numerous hospital-acquired nosocomial infections, including ventilator-associated pneumonia (VAP) [2], urinary tract infection (UTI) [3], meningitis [4] and septicemia [5]. Moreover, *A. baumannii* is also a member of the ESKAPE family of pathogens which consists of *Enterococcus faecium*, *Staphylococcus aureus*, *Klebsiella pneumoniae*, *A. baumannii*, *Pseudomonas aeruginosa* and *Enterobacter species*. The members of the ESKAPE family of pathogens are characterised by their increased resistance to some of the frequently used antibiotics, including penicillin, vancomycin and carbapenems [6]. Since the past 3 years, *A. baumannii* strains have developed resistance against a wide variety of antibiotics, including penicillin, cephalosporin and last expedient antibiotics such as carbapenems and polymyxins; these strains are generally referred to as multidrug [7] resistant *A. baumannii* (MDRAB) [8]. The World Health Organization (WHO) has classified *A. baumannii* as a priority I (critical) pathogen because it shows resistance against several classes of antibiotics [9]. According to a previous study, *A. baumannii* is responsible for 2 to 10% of all infections caused by gram-negative bacteria acquired in the USA and Europe. Unfortunately, multiple reports are confirming an increase in infections and mortality rates [10] connected with multidrug resistance *A. baumannii* (MDRAB) throughout the world [11]. Hence, it is an absolute necessity to identify promising drug-like molecules which can effectively treat the serious infections caused by *A. baumannii*.

Of the various metabolic pathways observed in MDRAB, the enzymes involved in peptidoglycan biosynthesis are an ideal and potential drug targets because of their relative dissimilarity [12] to any metabolic pathway taking place in *Homo sapiens* [13]. The cell wall is essential for the maintenance of overall shape and firmness of bacterial cells. Additionally, it also protects the cells from mechanical stress or bursting because of an imbalance in the osmotic pressure. The cell wall is made up of polymers of peptidoglycan (murein), which in turn are composed of sugars and amino acids [14] that form a mesh-like sheet over the cell membrane of most prokaryotes [15]. The enzymes involved in murein biosynthesis are indispensable for cell division amongst most bacterial species. There are eight members in the Mur family of enzymes, and they play pivotal role in the peptidoglycan biosynthetic pathway [16]. The UDP-N-acetylmuramoyl-L-alanine-D-glutamate ligase (MurD) belongs to the family of ADP forming ligases. A total of four ADP-forming ligases, namely MurC, MurD, MurE and MurF are required in the cytoplasm for peptidoglycan biosynthesis; they activate the congregation of peptide moiety by succeeding incorporations of L-alanine, D-glutamate, a diamino acid (lysine or diaminopimelate) and D-alanyl-D-alanine to UDP-N-acetylmuramic acid (UDP-MurNAc) [17, 18]. The principal function of MurD is to catalyse the addition of D-glutamate to its substrate UDP-N-acetylmuramoyl-L-alanine (UMA)

yielding UDP-N-acetylmuramoyl-L-alanyl-D-glutamate (UMAG) according to the following reaction [19]:



Moreover, the function of MurD is conserved across eubacteria, particularly *E. coli*. The three-dimensional structure of MurD ligase from *A. baumannii* is not yet available in Research Collaboratory Structural Bioinformatics - Protein Data Bank (RCSB – PDB) [20], but the crystal structure of MurD ligase from *Escherichia coli* has already been resolved at a high resolution of 1.66 Å (PDB ID - 4UAG) [21]. The MurD ligase from *E. coli* is expressed as a monomer of 437 amino acid residues and has a molecular weight of 47 kDa, which consists of three distinct globular domains formed from adjacent sections of the polypeptide chain. Domain 1 is responsible for the fixation of UDP moiety of UMA. The domain 2 (GTPase domain) is responsible for the attachment of ATP as well as the muramic acid and L-alanine moieties of UMA. The substrate (UMA) binds at the cleft present between domain 1 and the GTPase domain. The residues responsible for the attachment of UMA to the drug target protein include the following amino acid residues, namely Leu15, Thr16, Thr36, Arg37, Gly73, Asn138 and His183 [19]. In several studies, the Mur family of proteins, including MurD, have been suggested as a potential drug target against *A. baumannii* [22–26]. In the present study, we have investigated the sequential and structural properties of MurD ligase from *A. baumannii* and subsequently executed virtual high-throughput screening (vHTS) to identify novel drug-like molecules against it. We have employed various in silico techniques, including protein sequence analysis, homology modelling, virtual high-throughput screening (vHTS) and molecular dynamics (MD) simulations to achieve the results. Together with the results gathered from all these studies, we screened some promising drug-like candidates which could assist in the discovery and development of novel drug-like molecules for the successful treatment of hospital-acquired or nosocomial infections caused by *A. baumannii*.

Material and methods

Protein sequence analysis

The UniProt [27] database was used to retrieve the protein sequence of MurD from *A. baumannii* with the accession number: B0VDD5. ExPASy's (Expert Protein Analysis System) - ProtParam tool [28] was utilised to compute the various physicochemical properties of protein such as molecular weight, isoelectric point, amino acid composition, extinction coefficient, instability index and aliphatic index. Also, PSORTb [29] server was employed to predict the subcellular

localisation of MurD. Subsequently, the putative post-translational modifications or PTM sites (acetylation, glycosylation and phosphorylation) of MurD were predicted with the help of GPS-PAIL 2.0 [30], GLYCOPP v 1.0 [31] and MPSite [32] respectively. Also, the Conserved Secondary Structure Prediction (CSSP) web server was employed to predict the secondary structural composition (Helix, Sheet and Coil) of MurD ligase using the consensus approach [33]. The various methods which are employed by CSSP for secondary structure prediction include Discrimination of protein Secondary structure Class (DSC) [34], GOR IV [35], PSIPRED [36] and PHDsec [37]. The results obtained from CSSP are based on consensus prediction from the methods mentioned above, and hence they are reliable. Finally, the amino acid sequence of the MurD ligase was subjected to European Molecular Biology Open Software Suite (EMBOSS)-Antigenic program [38] to predict the possible antigenic sites.

Homology modelling and energy minimisation

The three-dimensional model of MurD ligase was generated by ModWeb server [39] using the crystal structure of MurD (PDB ID: 4UAG) from *E. coli* as the suitable structural template [21]. On default settings, it calculates a large number of models for each input sequence, if a template is available, and the model with the highest ModPipe quality score (MPQS) [39] and sequence identity per region is selected. Besides, we used ModWeb's slow [39] fold assignment method for the model creation. The modelled structure was analysed and superimposed with the template structure (PDB ID: 4UAG) using PyMOL [40] and Biovia Discovery Studio Visualizer [41]. Finally, the YASARA web server was employed to obtain the geometrically optimised and energy minimised model of MurD which was further used for virtual high-throughput screening (vHTS) and molecular dynamics (MD) simulation studies [42].

Model evaluation and binding site analysis

PROCHECK [43], ERRAT [44] and Verify 3D [45] programs were used to evaluate, compare the initial and optimised model of MurD ligase. These programs are available in a single web-based platform named as Structure Analysis and Verification Server (SAVES) (<https://servicesn.mbi.ucla.edu/SAVES/>). PROCHECK analyses the complete structural stereochemistry based on parameters like main chain ionic forces, types of internal angles and distances of interatomic interaction in virtue of Ramachandran plot [43]. ERRAT identifies and analyses valid and invalid segments of the modelled structure on behalf of their atomic interactions using statistical approaches [44]. The Verify-3D program estimates the relationship between the 3D and 1D amino acid

sequences [45]. The selection of the binding site residues was based on the substrate-binding pocket of the template structure (PDB ID: 4UAG) [21]. The template structure was aligned to the predicted model to identify the conserved and variable or non-conserved residues involved in the binding of UMA to MurD. The pairwise sequence alignment, followed by a structural superimposition, was performed using the "align" command present in PyMOL [40]. Additionally, we also used FATCAT [46] to perform the pairwise structural alignment. The root mean square deviation (RMSD) of the modelled MurD with reference to the template was also calculated using the align function in PyMOL [40].

Virtual high-throughput screening and molecular docking

Virtual high-throughput screening of a subset of Zinc database [47] against predicted MurD structure was completed on Drug Discovery@TACC web portal (<https://drugdiscovery.tacc.utexas.edu/>) [48] using AutoDock Vina [49] to identify the putative inhibitors against MurD ligase from *A. baumannii*. Non-site specific docking (blind or in-direct docking) was performed to identify all the possible binding sites with the size and coordinates of the grid box as follows: center_x = 36.25, center_y = -12.63, center_z = 22.70, size_x = 88.62, size_y = 73.48, size_z = 76.74 (see supplementary data). Blind docking is one of the excellent ways to identify all promising binding sites of a protein molecule [50–52]. The exhaustiveness for molecular docking calculations was set to 10. The web portal returned a list of the best 1000 ligand molecules ranked on the basis of their estimated binding affinities towards MurD.

Pharmacokinetics and drug-likeness

The best thousand ligand molecules showing maximum binding affinity towards MurD ligase were obtained using vHTS. Employing DataWarrior tool [53], the thousand ligands were filtered on the basis of Lipinski's rule of five [54] and different toxicological properties (carcinogenicity, mutagenicity, reproductive effects and irritating effects) [53]. Only 326 ligands passed these filters. Furthermore, the selected 326 ligands were screened on account of ADME (Absorption, Distribution, Metabolism and Excretion) properties using SwissADME [55]. SwissADME was employed to predict various parameters, including blood-brain barrier penetration (BBB), human intestinal absorption (HIA), aqueous solubility (AS), topological polar surface area (TPSA) and CYP2D6 inhibition. Out of 326, only 76 ligands passed the ADME filters. Finally, the four best ligands were selected based on the orientation of ligands in the binding site, key interacting residues and the number of intermolecular hydrogen bonds

(H-bonds) they were making with the active site residues of MurD ligase.

Molecular dynamics simulation

MD simulation overcomes the main limitation of the molecular docking studies, i.e. it considers both protein and ligands as completely flexible entities. It also mimics the physiological conditions much more effectively than molecular docking calculation [56]. The aqueous environment inside the cells, electroneutrality and physical parameters like temperature, pressure and volume are taken into account while performing MD simulations. These considerations make MD simulations much more statistically significant than molecular docking calculations. All of the selected MurD-ligand complexes and free MurD were subjected to MD simulations in an explicit solvent model. The simulations were performed using GROMACS 2019 [57] with GROMOS96 43A1 force field parameters [58]. An external program, PRODRG [59] was used to create the topologies (details of charge group, bond length, bond angle, proper and improper torsion angle, etc.) for the selected ligands. MD simulations of 100 ns were conducted for all of the MurD-ligand complexes and unbound MurD [60]. Counter-ions (positive or negative ions) were added to achieve electroneutrality of the systems. All of the structures were solvated within a 10 Å SPC/E (Extended Simple Point Charge model) water cube [61]. In the next step, the free protein and the protein-ligand complexes were energetically minimised in multiple steps utilising a steepest descent minimisation algorithm, where minimisation of the whole system, solvent molecules and the non-heavy atoms of the protein and protein-ligand complexes was eventually achieved. The energy minimisation was executed until the maximum force fell under 10 kJ/mol/nm. During the equilibration steps, the velocity rescaling (v-rescale) thermostat was used to maintain the temperature at 300 K. The equilibration was achieved in two phases, in the first phase, the number of particles, volume and temperature were kept constant (NVT), whereas in the second step, the number of particles, pressure and temperature were kept constant (NPT). All bonds were constrained using the LINCS (LINear Constraint Solver) algorithm [62] to allow a 2-fs time step. The systems were equilibrated for 50,000 steps at 300 K using isothermal-isochoric (NVT) ensemble and then for additional 50,000 steps at 300 K using isothermal-isobaric (NPT) ensemble to maintain the pressure at 1 bar. The Parrinello-Rahman barostat [63] was used to maintain the pressure at 1 bar. Cut-offs of 1 nm were used for the neighbour list, electrostatic interactions and van der Waals interactions. The Verlet cut-off scheme was applied for neighbour searching. The Particle-Mesh Ewald (PME) method [64] was employed for the estimation of long-range electrostatic interactions with an interpolation order of 4 and a grid spacing of 0.16 nm. Finally, production

MD runs of 100 ns (time step = 2 fs) were executed for MurD and the selected MurD-ligand complexes. The analysis of simulation trajectories was performed using GROMACS [57] and PyMOL [40]. Utilising the output trajectories of these MD simulations, various structural parameters like root mean square deviation (RMSD), root mean square fluctuations (RMSF), radius of gyration (Rg), solvent-accessible surface area (SASA) and intermolecular hydrogen bonds (H-bonds) were calculated.

Binding free energy calculations

In addition to global dynamic analysis, we calculated the binding free energies of the selected protein-ligand complexes employing MM/PBSA (molecular mechanics with Poisson-Boltzmann and surface area solvation) [65] method. It is one of the most reliable end-point methods to calculate the binding free energies for protein-ligand interactions. In this approach, the calculation of binding free energy relies on the following mathematical equation:

$$\Delta G_{\text{binding}} = \Delta E_{\text{mm}} + \Delta G_{\text{pol}} + \Delta G_{\text{np}} - T\Delta S \quad (1)$$

In this equation, $\Delta G_{\text{binding}}$ is the binding free energy of the protein-ligand complex, whereas, ΔE_{mm} depicts the gas-phase molecular mechanics energy, including bonded (bond, angle, dihedral and improper interactions) as well as non-bonded interactions {van der Waals (ΔE_{vdw}) and electrostatic contributions (ΔE_{ele})}. The ΔG_{pol} term describes the polar solvation free energy, and the ΔG_{np} showcases the non-polar solvation energy. Also, the $T\Delta S$ term represents the contribution of conformational entropy in a vacuum at temperature T . Since the MurD-ligand systems were nearly identical and they might have experienced identical entropy changes, the term $T\Delta S$ was ignored to reduce the computational expense [66]. Equation 1 can be rewritten as:

$$\Delta G_{\text{binding}} = \Delta E_{\text{bonded}} + \Delta E_{\text{non-bonded}} + \Delta G_{\text{pol}} + \Delta G_{\text{np}} - T\Delta S \quad (2)$$

It should be noted that in the single trajectory approach, the conformation of the free protein and the ligand-bound complexes are considered to be same. Thus, the term ΔE_{bonded} is always taken as zero [67]. Equation 2 can be rewritten as:

$$\Delta G_{\text{binding}} = \Delta E_{\text{vdw}} + \Delta E_{\text{ele}} + \Delta G_{\text{pol}} + \Delta G_{\text{np}} - T\Delta S \quad (3)$$

The components described in Eq. 3 (except the $T\Delta S$ part) were utilised to calculate the binding free energy values employing *g_mmpbsa* tool [68]. For the binding free energy calculations, 1000 snapshots (1 structure was captured every

20 ps) were captured from the final 20 ns of the stable trajectories of MurD-ligand complexes.

Results and discussion

Protein sequence analysis

The protein sequence of MurD from *A. baumannii* was retrieved from the UniProt database [27] with the accession number of B0VDD5. According to ExPASy's [28] ProtParam web server, the predicted amino acid length, molecular weight and theoretical isoelectric point were 455, 48.65 kDa and 6.14, respectively. Also, it had an instability index of 35.90, which categorised it as a stable protein. This result indicated that MurD ligase is thermodynamically stable. Additionally, the PSORTb [29] web server predicted MurD as a cytoplasmic protein. Besides, European Molecular Biology Open Software Suite (EMBOSS) antigenic web server [38] estimated twenty-one antigenic sites in MurD ligase (see supplementary data). Moreover, a recent study reported that the post-translational modifications (PTM) in ESKAPE pathogens are one of the promising routes for pathogenicity and virulence properties [69]. Therefore, in this study, we also employed several in silico tools to predict the PTM sites of MurD ligase. MPSite [32], GLYCOPP [31] and GPS-PAIL [30] were used to predict potential sites for phosphorylation, glycosylation and acetylation, respectively. MPSite [32] estimated a possible phosphorylation site at Ser453 residue. The GLYCOPP web server [30] indicated eleven *N*-linked glycosylation and none *O*-linked glycosylation (see supplementary data). Also, GPS-PAIL [30] suggested three acetylation sites in MurD ligase (see supplementary data). In addition to this, the Conserved Secondary Structure Prediction (CSSP) web server [33] revealed the percentage of alpha helices and beta sheets found to be 40.65% and 13.18%,

respectively. A total of 16 helices and 12 beta-sheets were computed by this web server.

Homology modelling and energy minimisation

The 3D model of MurD ligase from *A. baumannii* has not yet been reported. Predicting the 3D structure of a protein molecule is crucial to explore its function [70], and it also enables us to identify potential lead or drug-like candidates against it utilising the structure-based drug design (SBDD) or drug repurposing approaches [71]. In this case, ModWeb [39] used the experimentally determined crystal structure of MurD ligase from *E. coli* (PDB ID: 4UAG) [21] to create the homology model of MurD from *A. baumannii*. The template was resolved at a resolution of 1.66 Å. The structural template had the query coverage and percentage of sequence identity of 94% and 44.68%, respectively. In the template structure (PDB ID: 4UAG), there are three globular domains, and the substrate-binding site (UMA binding site) is present between domain 1 and domain 2. Domain 1 includes residues 1–93, domain 2 (GTPase domain) includes residues 94–298 and the domain 3 comprises residues 299–437. The residues involved in the fixation of UMA to MurD include Leu15, Thr16, Thr36, Arg37, Gly73, Asn138 and His183 residues [19]. As the template, the model (Fig. 1) obtained from ModWeb's server [39] had three distinct globular domains. A pairwise structural alignment between the predicted MurD ligase and the structural template revealed the MurD model sharing several conserved amino acid residues with the template structure. The FATCAT web server (http://fatcat.godziklab.org/fatcat/fatcat_pair.html) computed that the two structures were significantly similar with *P* value of 0.00e+00. The models had 425 equivalent positions with an RMSD of 0.58 Å without twists. The conserved amino acid residues included the residues present at the UMA binding site

Fig. 1 The 3D model of MurD with illustration of domain I (1–101) (red), domain II (102–309) (purple) and domain III (310–454) (cyan) and the zoomed view is showing the residues at the UMA binding site

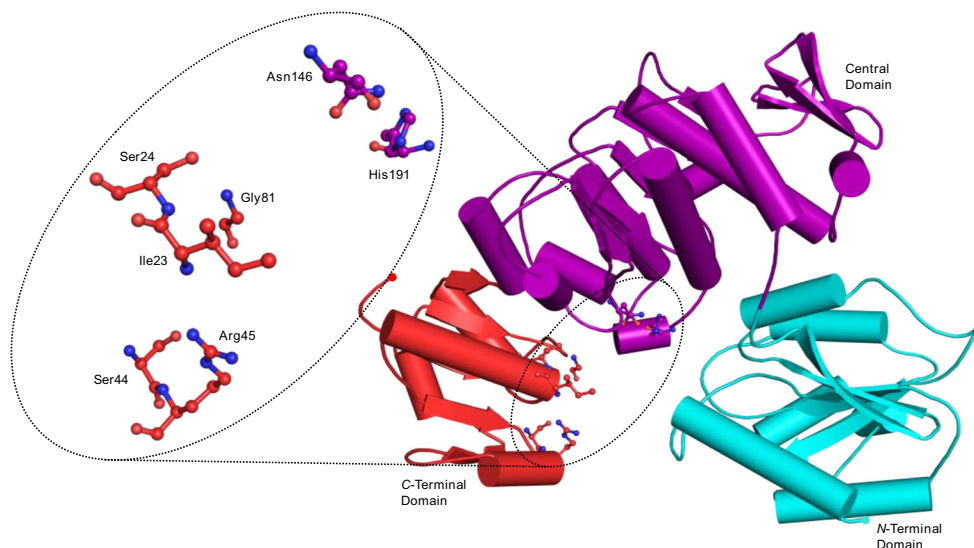
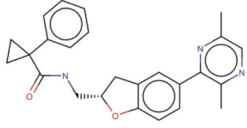
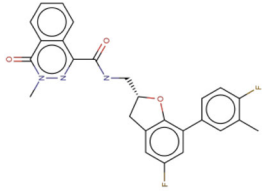
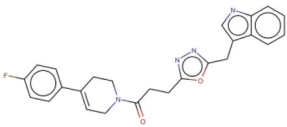
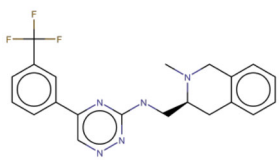


Table 1 Estimated binding affinities and estimated inhibition constants of the selected ligands along with their chemical schemes

S/No	Accession No.	Estimated Binding Affinity (kcal/mol)	Estimated Inhibition constant (nM)	Molecular formula	2D Structure
1	ZINC12055135	-10.1	0.39	C ₂₅ H ₂₅ N ₃ O ₂	
2	ZINC12097291	-10.6	0.16	C ₂₆ H ₂₁ N ₃ O ₃ F ₂	
3	ZINC12454357	-10.2	0.33	C ₂₅ H ₂₃ N ₄ O ₂ F	
4	ZINC19221101	-10.3	0.28	C ₂₁ H ₂₀ N ₅ F ₃	

present between domains 1 and 2. The UMA binding site of the predicted MurD model includes Ile23, Ser24, Ser44, Arg45, Gly81, Asn146 and His191 amino acid residues.

Out of these seven residues, the last four residues (Arg45, Gly81, Asn146 and His191) are conserved in both the structures. In the modelled structure, domain 1 consists of residues 1–101, domain 2 consists of residues 102–309 and domain 3 consists of residues 310–454. According to PDBsum [72] web server, the MurD ligase has a $\beta\alpha\beta$ architecture, and the

secondary structure of the protein is comprised of 18.7% of strands, 28.4% of alpha-helices, 4.7% of 3_{10} helices and 48.2% of other secondary structure elements (see supplementary data). Energy minimisation of the modelled structure was performed using YASARA web server [42]. More importantly, 91.4% of the residues of modelled structure were observed in the most favoured region of the Ramachandran plot. The modelled structure had an ERRAT quality factor of 95.632 and Verify 3D score of 97.52%. The RMSD value of the

Table 2 Lipinski's rule of five and drug-likeness properties of the selected four ligands

S/No..	Ligands ID	MW (≤ 500)	cLogP (≤ 5)	rBonds (≤ 10)	HBA (≤ 10)	HBD (≤ 5)	DL
1.	ZINC12055135	419.651	2.278	6	5	4	-0.47607
2.	ZINC12097291	485.657	1.2087	5	6	4	-3.1954
3.	ZINC12454357	452.656	2.4732	7	6	4	-0.3595
4	ZINC19221101	417.562	2.6481	5	5	4	-6.7865

MW molecular weight, cLogP lipophilicity, rBonds rotatable bond is a measure of molecular flexibility of a compound, HBD hydrogen bond donor, HBA, hydrogen bond acceptor, DL drug-likeness

Table 3 List of the selected four ligands with their toxicity parameters

S/ No.	Zinc code	Carcinogenic	Mutagenic	Reproducibility	Irritant
1	ZINC12055135	Non-carcinogens	None	None	None
2	ZINC12097291	Non-carcinogens	None	None	None
3	ZINC12454357	Non-carcinogens	None	None	None
4	ZINC19221101	Non-carcinogens	None	None	None

structure superimposition of modelled MurD with the template structure was 0.503 Å, which indicated the reliability of the predicted model based on the satisfaction of spatial restraints [39]. The optimised MurD model was deposited into Protein Model Data Base (<http://srv00.recas.ba.infn.it/PMDB/user/search.php>) with the accession number of PM0083163.

vHTS

In rational drug design, structure-based virtual screening (SBVS) is a principal tool to elucidate protein-ligand interactions [73] followed by identification of potential and promising drug-like candidates. Molecular docking aims to predict the best binding orientation of ligands into the catalytic pocket of a protein molecule with a known three-dimensional structure [74]. Comprehending the binding and interactions of small molecules with a protein or other macromolecule is of great significance in the field of drug designing and discovery process [75]. Moreover, molecular docking algorithms can execute quantitative prediction of estimated binding affinities (ΔG), estimated inhibition constants (K_i) and rank the docked ligands based on their binding affinity towards the protein molecule. The potential binding pocket residues of MurD include Ile23, Ser24, Ser44, Arg45, Gly81, Asn146 and His191 amino acid residues. To inhibit the target protein (MurD), the molecules obtained from vHTS should be oriented in the aforementioned binding pocket. The SBVS of MurD ligase was performed using DrugDiscovery@TACC web portal [48] which employs AutoDock Vina for its docking calculations [49]. The docking procedure was applied to the entire protein without imposing the binding site restrictions (blind docking or non-site-specific docking). A ZINC library of ~642,759 commercially available

molecules was screened against MurD, and the best 1000 ligands showing maximum binding affinity towards drug target protein were subjected to further analyses.

Physicochemical properties and ADMET analysis

After obtaining the best 1000 ligands from the DrugDiscovery@TACC web portal [48], they were further subjected to DataWarrior tool [53] for the evaluation of physicochemical properties such as Lipinski's rule of five, drug-likeness and toxicity (carcinogenicity, mutagenicity, reproductive effects and irritating effects).

The permitted values for drug-likeness, rotatable bonds and toxicity were ≤ 5 , ≤ 10 and none, respectively. Out of the 1000 ligands, only 326 passed these physicochemical parameters and were further subjected to SwissADME [55] for ADME (Absorption, Distribution, Metabolism and Excretion) analysis. Pharmacokinetics refers to the study of the interactions of a drug molecule inside a living body. It defines the onset of action, residence time and intensity of a drug in vivo. The pharmacokinetics of the drug-like molecules can be understood through absorption, distribution, metabolism, excretion and toxicity parameters. We employed SwissADME [55] to compute the ADME parameters, including blood-brain barrier penetration (BBB), human intestinal absorption (HIA), Octanol-water partition coefficient (cLogP), aqueous solubility (AS), topological polar surface area (TPSA) and Cytochrome P450 2D6 (CYP2D6) inhibition. The ligands which were HIA+, BBB+, soluble in the aqueous medium, having TPSA smaller than 100 nm² and non-inhibitor of CYP2D6 were selected for further screening.

Table 4 ADME profiles of the selected four ligands

S/ No.	Zinc code	HIA	BBB	Consensus Log P	TPSA	Aqueous solubility (AS)	CYP450 2D6 inhibitor
1.	ZINC12055135	HIA+	BBB+	3.27	65.55	Soluble	Non-inhibitor
2	ZINC12097291	HIA+	BBB+	3.06	76.99	Soluble	Non-inhibitor
3	ZINC12454357	HIA+	BBB+	3.23	68.79	Soluble	Non-inhibitor
4	ZINC19221101	HIA+	BBB+	3.29	51.36	Soluble	Non-inhibitor

HIA human intestinal absorption, BBB blood-brain barrier, Consensus Log P Octanol-water partition coefficient, TPSA total polar surface area, CYP2D6 cytochrome P4502D6

Table 5 Interaction details of the selected ligands with MurD

S/ Ligands No.	HB	<i>D</i> (Å)	Pi-SR	<i>D</i> (Å)	vdW/ISR
1	ZINC12055135 Ile23Ser24Lys123Asn146Tyr440	2.892.182.112.362.69	Ile23Pro80Phe169His191Lys330Tyr440	4.515.424.924.874.934.07, 5.21	Gly22, Gly25, Arg45, Ser79, Gly81, Ser124, Ser167, Asp190, Thr332, Asn333
2	ZINC12097291 Lys123Ser124Asn146Tyr440	2.69, 1.982.202.322.20	Glu165Phe169His191Lys330Tyr440	4.41, 4.234.824.905.10, 5.325.06	Pro80, Gly81, Ser120, Asn121, Ala122, Leu147, Gly148, Ser167, Phe434, Ser439, Asn441
3	ZINC12454357 Lys123Asn146Lys364Tyr440	2.192.172.922.37	Lys123His191Lys330Phe434 Tyr440	4.994.984.424.60, 4.984.07, 4.444.91	Gly81, Ser120, Asn121, Ala122, Ser124, Ser167, Phe169, Arg194, Arg313, Thr332, Asn333
4	ZINC19221101 Ala122Lys123Ser124Asn146	2.842.682.512.63	Lys123Glu165Lys330Phe434 Tyr440	4.964.564.664.41, 3.724.74	Asn121, Phe169, His191, Arg313, Thr332, Lys364

HB hydrogen bond interaction, *D* distance, *Pi-SR* Pi-interaction sharing residues, *vdW* van der Waals interaction

Out of 326 ligands, only 76 passed these ADME filters. Since non-site specific or blind docking was performed, ligands were also binding to sites other than the substrate-binding pocket. Only those ligands were selected, which were present within the substrate-binding pocket and additionally, the orientation and interaction of the ligands inside the catalytic pocket were also analysed. In the end, four ligands (ZINC12055135, ZINC12097291, ZINC12454357 and ZINC19221101) having the most appropriate binding site orientation and the maximum number of intermolecular hydrogen bonds (H-bonds) with the binding site residues were selected and subjected to MD simulations. The estimated binding affinities (ΔG) for ZINC19221101, ZINC12055135, ZINC12097291 and ZINC12454357 were -10.3 kcal/mol, -10.1 kcal/mol, -10.6 kcal/mol and -10.2 kcal/mol, respectively (Table 1). The drug-likeness properties, toxicity parameters and ADME profiles of the top MurD-ligand complexes are summarised in Tables 2, 3 and 4, respectively. The interaction details of the selected MurD-ligand complexes are summarised in Table 5.

Interaction studies of MurD-ligand complexes

The estimated binding affinity (ΔG) of ZINC19221101 for MurD was -10.3 kcal/mol, and the estimated inhibition constant (K_i) was 0.28 nM. The ligand was interacting with the protein molecule through hydrogen bonding, pi interactions and van der Waals interactions (Fig. 2 and Table 5). The ligand was observed interacting with Ala122, Lys123, Ser124 and Asn146 residues (catalytically conserved residue in both template and target structures) via hydrogen bonding interactions. It was also found interacting with Lys123, Glu165, Lys330, Phe434 and Tyr440 amino acid residues utilising pi interactions. Also, ZINC19221101 was recorded interacting with Asn121, Phe169, His191 (catalytically conserved residue), Arg313, Thr332 and Lys364 amino acid residues via van der Waals interactions. The 2D and 3D MurD-ligand interaction diagrams were made using BIOVIA Discovery Studio [41] and PyMOL [40] programs, respectively.

The estimated ΔG for MurD-ZINC12055135 complex was observed to be -10.1 kcal/mol, and the estimated K_i was 0.39 nM. This ligand was also found interacting with Ile23, Ser24, Lys123, Asn146 and Tyr440 residues via hydrogen bonding interactions (Fig. 3 and Table 5). Out of these residues, Ile23, Ser24 and Asn146 are catalytically conserved residues. Besides, the ligand also interacted with Ile23 (catalytically conserved residue), Pro80, Phe169, His191 (catalytically conserved residue), Lys330 and Tyr440 via pi interactions. Finally, the ligand was observed to be interacting with Gly22, Gly25, Arg45 (catalytically conserved residue), Ser79, Gly81 (catalytically conserved residue), Ser124, Ser167, Asp190, Thr332 and Asn333 using van der Waals interactions.

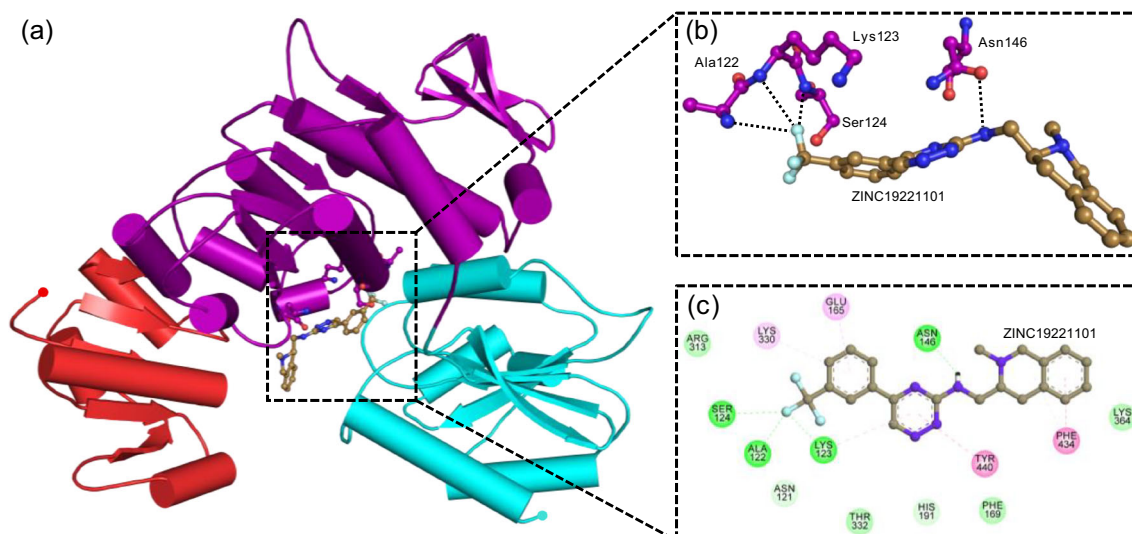


Fig. 2 (a) Interaction of ZINC19221101 (sand colour) with MurD (domain I—red, domain II—purple, domain III—cyan). (b) 3D representation of MurD active site residues interacting with ZINC19221101 (sand colour). (c) 2D representation of MurD active site residues interacting

with ZINC19221101 (sand colour) via van der Waals interactions (slightly green colour), hydrogen bonds (dark green colour) and pi interactions (light pink colour)

The estimated ΔG of ZINC12097291 for MurD was computed to be -10.6 kcal/mol, and the estimated K_i was 0.16 nM. The ligand was found interacting with Lys123, Ser124, Asn146 (catalytically conserved residue) and Tyr440 via hydrogen bonding interactions (Fig. 4 and Table 5). Also, the ligand utilised pi interactions to interact with Glu165, Phe169, His191 (catalytically conserved residue), Lys330 and Tyr440. Furthermore, ZINC12097291 was found interacting with Pro80, Gly81 (catalytically

conserved residue), Ser120, Asn121, Ala122, Leu147, Gly148, Ser167, Phe434, Ser439 and Asn441 via van der Waals interactions.

The estimated ΔG of MurD-ZINC12454357 was computed to be -10.2 kcal/mol, and the estimated K_i was 0.33 nM. The ligand was found interacting with Lys123, Asn146 (catalytically conserved residue), Lys364 and Tyr440 via hydrogen bonding interactions (Fig. 5 and Table 5). Also, it was observed interacting with Glu165,

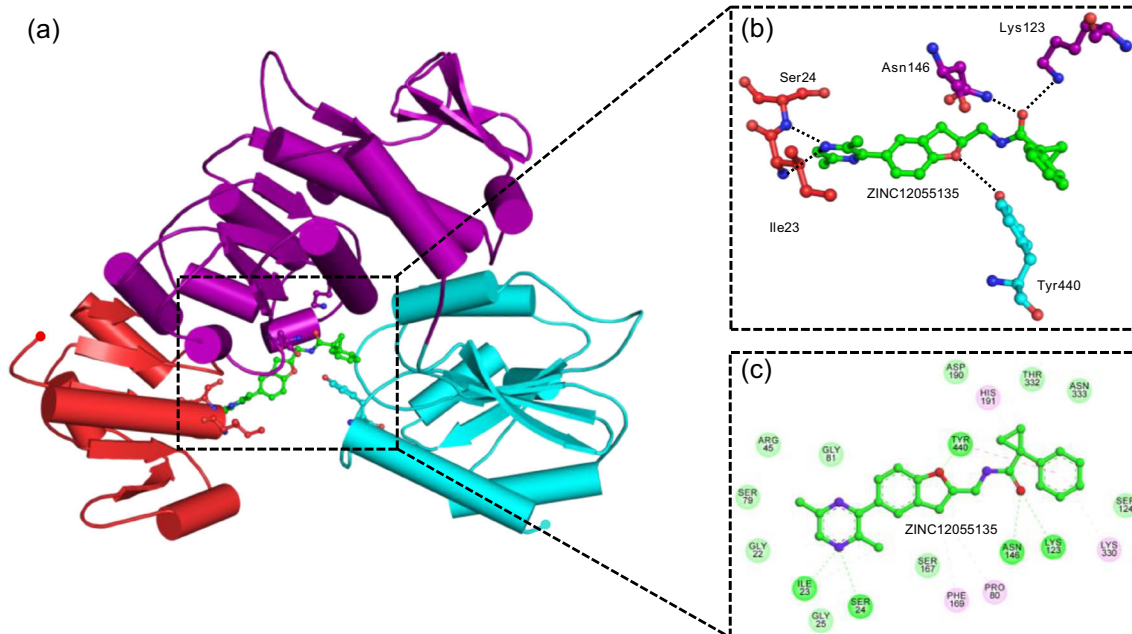


Fig. 3 (a) Interaction of ZINC12055135 (green colour) with MurD (domain I—red, domain II—purple, domain III—cyan). (b) 3D representation of MurD active site residues interacting with ZINC12055135 (green colour). (c) 2D representation of MurD active site residues

interacting with ZINC12055135 (green colour) via van der Waals interactions (slightly green colour), hydrogen bonds (dark green colour) and pi interactions (light pink colour)

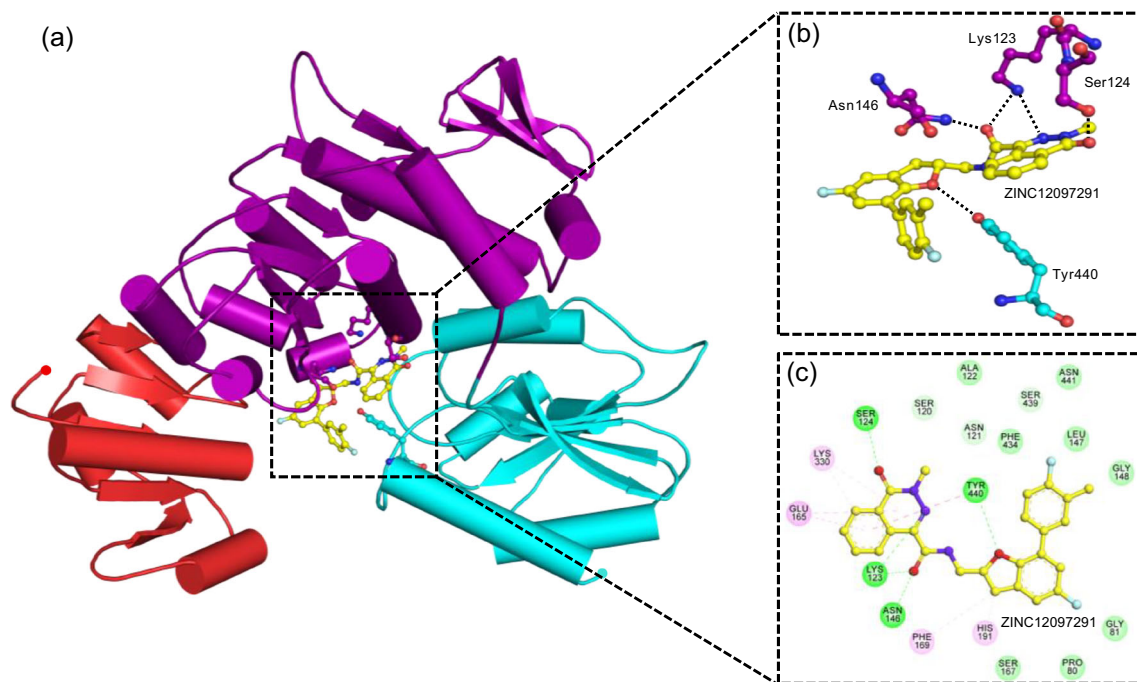


Fig. 4 (a) Interaction of ZINC12097291 (yellow colour) with MurD (domain I—red, domain II—purple, domain III—cyan). (b) 3D representation of MurD active site residues interacting with ZINC12097291 (yellow colour). (c) 2D representation of MurD active site residues interacting

with ZINC12097291 (yellow colour) via van der Waals interactions (slightly green colour), hydrogen bonds (dark green colour) and pi interactions (light pink colour)

Phe169, His191 (catalytically conserved residue) and Lys330 using pi interactions. Finally, ZINC12454357 was also found interacting with Pro80, Gly81 (catalytically conserved residue), Ser120, Asn121, Ala122, Leu147,

Gly148, Ser167, Phe434, Ser439 and Asn441 residues via van der Waals interactions.

As evident from MurD-ligand binding analysis, all four ligands were actively interacting with the catalytic site

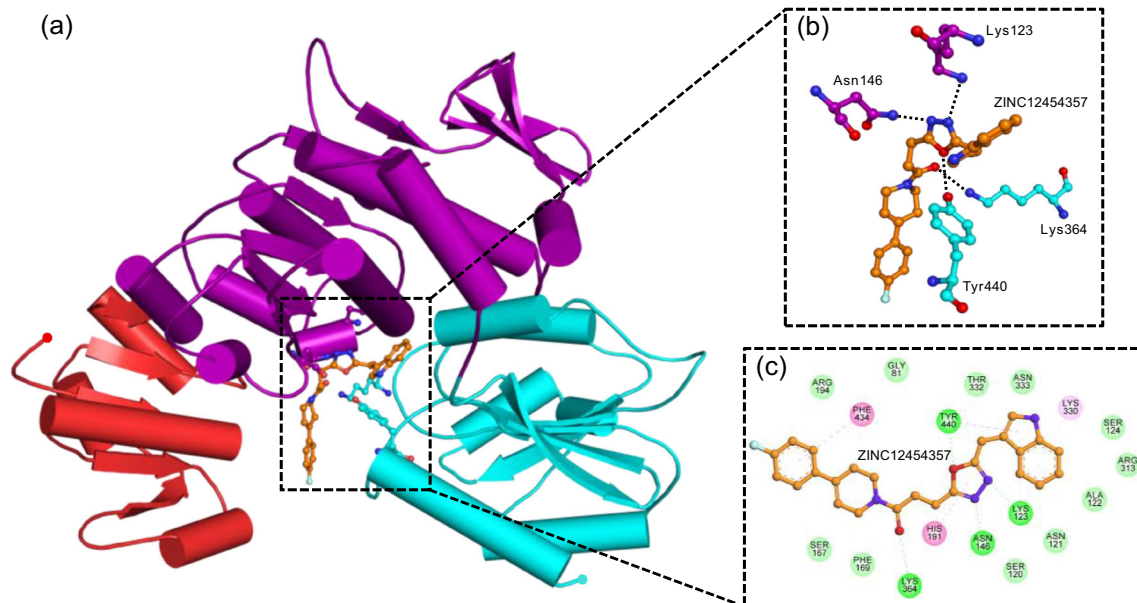


Fig. 5 (a) Interaction of ZINC12454357 (orange colour) with MurD (domain I—red, domain II—purple, domain III—cyan). (b) 3D representation of MurD active site residues interacting with ZINC12454357 (orange colour). (c) 2D representation of MurD active site residues

interacting with ZINC12454357 (orange colour) via van der Waals interactions (slightly green colour), hydrogen bonds (dark green colour) and pi interactions (light pink colour)

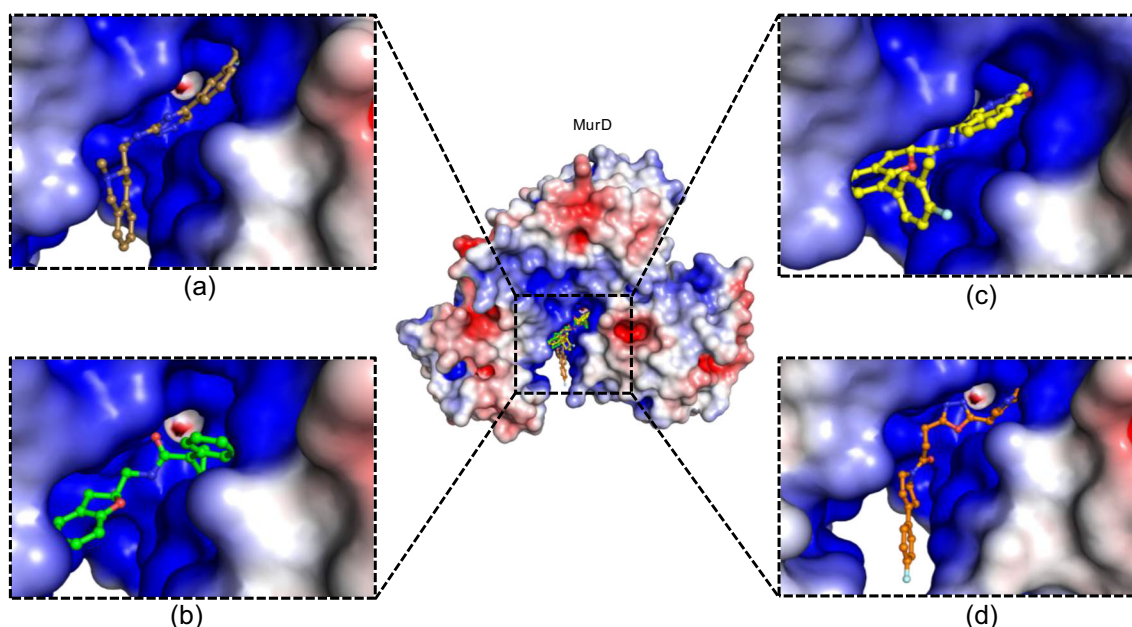


Fig. 6 The electrostatic surface potential map of (a) ZINC19221101 (sand colour), (b) ZINC12055135 (green colour), (c) ZINC12097291 (yellow colour) and (d) ZINC12454357 (orange colour) bound to MurD. The zoomed view is representing the active site cleft

residues with $\Delta G < -10.1$ kcal/mol and $K_i < 0.4$ nM. Also, all four ligand molecules were highly hydrophobic because of the aromatic rings, and all four of them participated in at least one hydrogen bond with the conserved UMA binding site residues. ZINC12055135 was H-bonded to three UMA binding site residues, including Ile23, Ser24 and Asn146 residues. The other three ligands were involved in H-bonding with only one conserved UMA binding site residue (Asn146), but they did participate in other kinds of intermolecular interactions (π interactions and van der Waals interactions) with the conserved residues. Besides, these interactions indicated that the selected ZINC ligands had substantial binding affinities towards MurD ligase. Generally, a higher number of hydrogen bonds, π interactions and van der Waals interactions depict a strong binding between the protein and ligand molecules, and it is also crucial in selecting promising candidates for drug discovery and development process. Moreover, multiple *in silico* studies have classified the Mur family of enzymes as potential drug targets against *A. baumannii* [22]. Structure-based virtual screening approach was employed to identify potential lead molecules against multidrug-resistant *A. baumannii*, which provided vital insights towards understanding the various structural aspects like predominant binding orientation, key intermolecular interactions, key interacting residues, the estimated binding affinities and estimated inhibition constants [23, 24, 26, 76]. Furthermore, the electrostatic surface potential analysis revealed that the pH of the substrate-binding cleft of the predicted MurD model was highly basic. Also, all four ligands appeared to be optimally oriented and entirely blocking the substrate-binding cleft of MurD ligase (Fig. 6).

Molecular dynamics simulations

Molecular dynamics (MD) simulations are performed to study the atomic transitions of entire macromolecules on a given time scale. It can also be utilised to evaluate the strength, stability, interaction pattern and properties of protein-ligand interactions. Furthermore, MD simulations can also be used to elucidate dynamic conformational changes a macromolecule experience in hydrophilic cellular environments. Various structural parameters, including RMSD, RMSF, Rg, SASA and intermolecular H-bonds, were calculated. To assess the conformational stability, compactness, folding characteristics and intermolecular interactions of protein-ligand complexes, MD simulations of 100 ns were performed for both free and ligand-bound MurD forms.

Root mean square deviation

RMSD is an essential tool to estimate the conformational stability of protein and protein-ligand complexes as a function of time. The free MurD stabilised at 10 ns and maintained it until 35 ns, after which the RMSD started to spike, and it reached its peak value at around 40 ns (Fig. 7a). The free protein started to stabilise again at around 40 ns, and this time, it was maintained it until the end of the simulation period with a few minor variations. In contrast, the MurD-ZINC19221101 complex stabilised at around 10 ns, and it maintained its structural stability until the end of the MD simulation period. The MurD-ZINC12454357 complex also gained its stability around 10 ns and preserved it until the end of the 100-ns MD simulation. The MurD-ZINC12097291 complex also

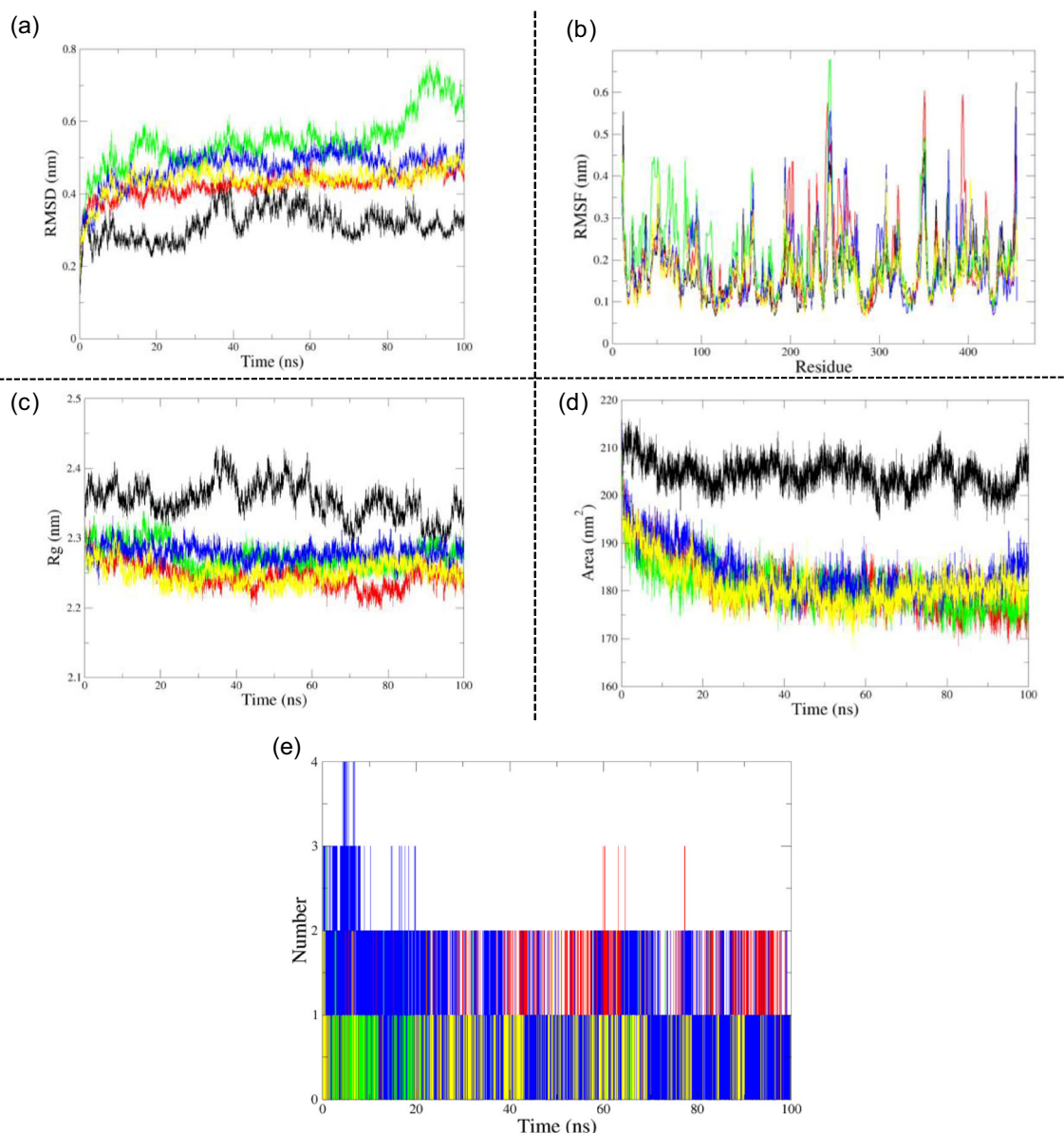


Fig. 7 Analysis of molecular dynamics simulation results of free MurD (black), MurD-ZINC19221101 complex (red), MurD-ZINC12055135 complex (green), MurD-ZINC12097291 complex (blue) and MurD-ZINC12454357 complex (yellow). (a) Root Mean Square Deviation

(RMSD). (b) Root Mean Square Fluctuation (RMSF). (c) Radius of gyration (Rg). (d) Solvent-Accessible Surface Area (SASA). (e) Intermolecular H-bonds

gained its stability around 10 ns and preserved it until the end of the simulation period except for the minor variations at 50 and 80 ns. Finally, the MurD-ZINC12055135 complex achieved its stability at around 20 ns and maintained it until 80 ns. After 80 ns, the deviations started to spike and achieved the maximum value at around 90 ns and then it started to drop. The MurD-ZINC19221101 and MurD-ZINC12454357 complexes were closest to the free MurD structure and were the most stable ones out of the all four protein-ligand complexes. The average RMSD values for free MurD, MurD-ZINC19221101, MurD-ZINC12055135, MurD-

ZINC12097291 and MurD-ZINC12454357 were 0.3178 nm, 0.4243 nm, 0.5447 nm, 0.4731 nm and 0.4377 nm, respectively.

Root mean square fluctuation

RMSF is the measure of average fluctuations a protein molecule experiences under physiological conditions. It is also used to understand the flexibility and rigidity of protein and protein-ligand complexes. It is measured for the C-alpha atom of each amino acid residue representing a protein molecule. In the case of MurD, the maximum

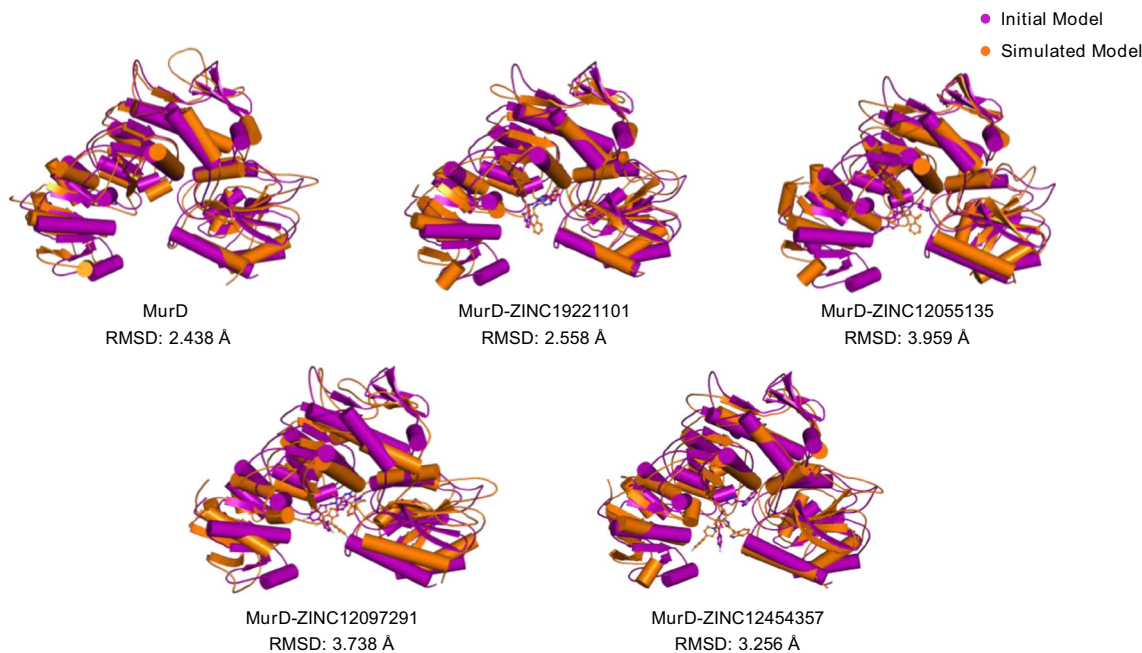


Fig. 8 Structural superimposition of the initial (purple colour) and MD simulated (orange colour) MurD and its ligand-bound complexes

fluctuations were observed in the loop dominant regions (mostly in the second GTPase domain) (Fig. 7b). The flexibility of the loop regions allows the ligands to enter the protein molecule and bind at the substrate-binding site. Also, all ligands except ZINC12454357 appeared to be maximising the fluctuations of MurD. The MurD-ZINC12055135 complex was showing the maximum variations with respect to the free MurD structure, whereas the MurD-ZINC12454357 complex had the least fluctuations compared with the free protein. The average RMSF values for the free MurD, MurD-ZINC19221101, MurD-ZINC12055135, MurD-ZINC12097291 and MurD-ZINC12454357 complexes were 0.1694 nm, 0.1877 nm, 0.2052 nm, 0.1840 nm and 0.1667 nm, respectively.

Radius of gyration

The radius of gyration (Rg) is an important structural parameter to elucidate the equilibrium conformation, compactness and

folding characteristics of protein and protein-ligand complexes. Rg indicates whether the binding of a ligand molecule stabilises the protein structure or not. The Rg of MurD-ZINC12454357 and MurD-ZINC19221101 complexes were almost the same, indicating that both of these ligands preserved MurD’s conformation equally well (Fig. 7c). Besides, the Rg data showed that all four MurD-ligand complexes were structurally more compact with improved folding behaviour than the free MurD structure, and the graph for all of the MurD-ligand complexes was very stable with minimum variations. The average Rg for the free MurD, MurD-ZINC19221101, MurD-ZINC12055135, MurD-ZINC12097291 and MurD-ZINC12454357 complexes were 2.355 nm, 2.246 nm, 2.274 nm, 2.278 nm and 2.249 nm, respectively.

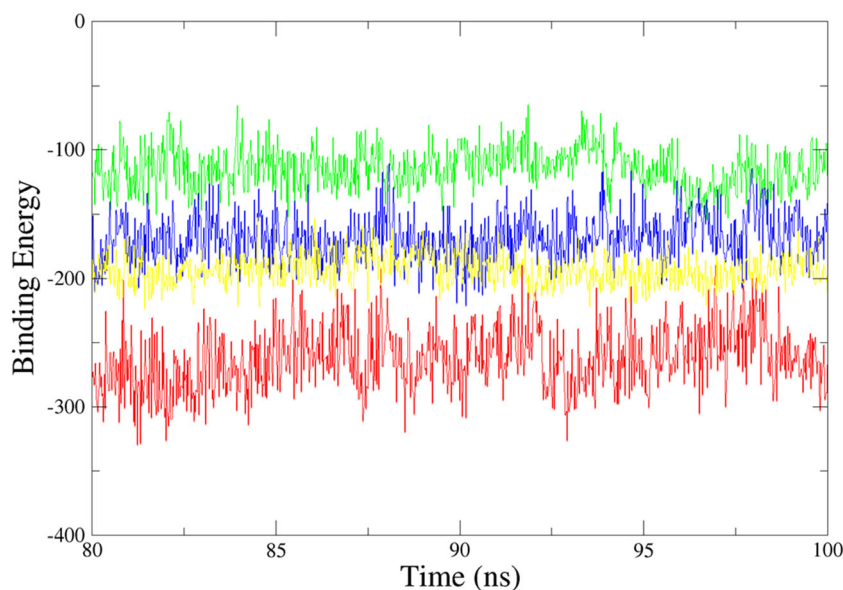
Solvent-accessible surface area and intermolecular H-bonds

SASA is employed to describe a change in the solvent behaviour of a protein molecule resulting from the conformational

Table 6 Contribution of individual energy components involved in complex formation between MurD and the top lead molecules

S. No.	System	van der Waals energy (kcal/mol)	Electrostatic energy (kcal/mol)	Polar solvation energy (kcal/mol)	SASA energy (kcal/mol)	Binding free energy (kcal/mol)
1.	MurD-ZINC19221101	- 54.5 ± 2.8	- 51.4 ± 5.1	47.6 ± 7.3	- 4.4 ± 0.1	- 62.6 ± 5.6
2.	MurD-ZINC12055135	- 40.8 ± 5.4	- 0.8 ± 1.5	18.2 ± 7.2	- 3.8 ± 0.5	- 27.2 ± 3.6
3.	MurD-ZINC12097291	- 67.9 ± 2.9	- 7.0 ± 1.2	39.9 ± 3.6	- 5.2 ± 0.2	- 40.2 ± 4.2
4.	MurD-ZINC12454357	- 55.0 ± 2.3	- 1.5 ± 0.9	15.0 ± 2.2	- 4.6 ± 0.2	- 46.1 ± 2.6

Fig. 9 Binding free energy analysis results of MurD-ZINC19221101 complex (red), MurD-ZINC12055135 complex (green), MurD-ZINC12097291 complex (blue) and MurD-ZINC12454357 complex (yellow) (energy values expressed in kJ/mol)



changes it may experience upon binding to a ligand. In the case of MurD, all four protein-ligand complexes were capable of decreasing the SASA in comparison with the free protein (Fig. 7d). The SASA of all four MurD-ligand complexes stabilised at around 20 ns and preserved it until the end of the MD simulation cycle. The average SASA values for the free MurD, MurD-ZINC19221101, MurD-ZINC12055135, MurD-ZINC12097291 and MurD-ZINC12454357 complexes were 204.703 nm², 181.239 nm², 180.856 nm², 183.623 nm² and 181.115 nm², respectively. In comparison with free MurD, the average SASA values of all of the ligand-bound forms decreased slightly, which indicated that these ligand molecules induced conformational changes in the protein structure.

The number of H-bonds a ligand molecule forms with the protein molecule is a vital parameter during MD simulations. A higher number of H-bonds generally refer to a substantial binding affinity of a ligand towards the protein molecule. Out of all four MurD-ligand complexes, the maximum instances of H-bonds were observed in the case of MurD-ZINC12097291 complex, whereas the minimum instances were observed in the case of MurD-ZINC12055135 complex (Fig. 7e). Also, MurD-ZINC12097291 complex was found to be interacting with the maximum number of H-bonds (four H-bonds), whereas the MurD-ZINC12055135 complex was interacting with the least number of H-bonds (one H-bond).

Comparative structural analysis of modelled and simulated MurD structures

The structures of modelled MurD and simulated MurD having the lowest potential energies were analysed using the align structural superimposition function available in PyMol (Fig. 8) [40]. The minimum potential energies of MurD, MurD-ZINC19221101, MurD-ZINC12055135, MurD-

ZINC12097291 and MurD-ZINC12454357 were found to be $-1,225,688.125$ kJ/mol (at 60.89 ns), $-1,192,148.375$ kJ/mol (at 10.78 ns), $-1,193,003.000$ kJ/mol (at 0 ns), $-1,192,378.500$ kJ/mol (at 19.38 ns) and $-1,193,252.625$ kJ/mol (at 60.79 ns), respectively. The RMSD of the MurD-ligand complexes were observed to be higher than that of the free protein (2.438 Å), but none of the ligands deviated MurD's confirmation too significantly. Moreover, the structural superimposition analysis also depicted that the ligands were appropriately oriented in the catalytic site of MurD during the MD simulations. The structural superimposition of MurD-ZINC19221101, MurD-ZINC12055135, MurD-ZINC12097291 and MurD-ZINC12454357 revealed RMSDs of 2.558 Å, 3.959 Å, 3.738 Å and 3.256 Å, respectively.

After analysing the MD simulation data, it can be confidently said that ZINC19221101 and ZINC12454357 consistently performed better than ZINC12055135 and ZINC12097291 and are probably the better candidates for inhibiting the action of MurD ligase. These two ligands performed better than the other two in almost all aspects (RMSD, Rg and SASA) of MD simulation except the intermolecular H-bonds in which ZINC12097291 was better than all other ligands.

Binding free energy analysis

Binding free energy analysis aimed to calculate the energies that were associated with the binding of ZINC ligands to MurD during the MD simulations. A precise estimation of binding free energies of the protein-ligand complexes is amongst the most critical aspects of understanding protein-ligand interactions. The binding free energies were estimated for all four selected MurD-ligand complexes (MurD-ZINC19221101, MurD-ZINC12055135, MurD-

ZINC12097291 and MurD-ZINC12454357) utilising the MM/PBSA approach. A total of 1000 snapshots or conformations were captured from the final 20-ns stable MD trajectories with an interval of 20 ps for each system. The binding free energies for MurD-ZINC19221101, MurD-ZINC12055135, MurD-ZINC12097291 and MurD-ZINC12454357 were estimated to be -62.6 ± 5.6 kcal/mol, -27.2 ± 3.6 kcal/mol, -40.2 ± 4.2 kcal/mol and -46.1 ± 2.6 kcal/mol, respectively (Fig. 9 and Table 6).

These results revealed strong interactions between MurD-ligand complexes, especially between MurD-ZINC19221101 and MurD-ZINC12454357. In all of the cases, the van der Waals energies were prime contributors to the binding free energies. The electrostatic and SASA energies were also found to be sufficiently dominant. Conversely, polar solvation energies unfavourably contributed to the binding free energies in all MurD-ligand complexes. Furthermore, the results obtained from binding free energy analysis corroborated with the results obtained from global dynamic analysis. Together with the results obtained from all these analyses, we propose that ZINC19221101 and ZINC12454357 molecules are worth further investigations.

Conclusions

The sporadic outbreak of healthcare-associated infections (ventilator-associated pneumonia, urinary tract infection, etc.) associated with *A. baumannii* has made it compulsory to identify new therapeutic options against it [77–80]. In a few cases, the mortality rate can even surge as high as 35% [65]. The present study was aimed at predicting novel drug-like or lead-like compounds acting against an essential cell wall biosynthesis enzyme. In the current study, MurD ligase was homology modelled and subjected to vHTS against a library of 0.6 million commercially available molecules from the ZINC database. The best thousand ligands obtained from vHTS were screened against various parameters, and subsequently, the best four ZINC ligands were chosen for further validations employing MD simulations and binding free energy calculations. Finally, the results of MD simulations and binding free energy analysis depicted that two (ZINC19221101 and ZINC12454357) of the best four ligands could be considered as lead molecules for drug discovery against *A. baumannii*. However, computational studies are limited in a way that they cannot fully mimic the physiological conditions [81, 82]; therefore, further experimental investigations are required to confirm the activity of these ligands against *A. baumannii*. Although additional validations are required, the results of this study are encouraging and may expedite the efforts to develop effective antibiotics against *A. baumannii*.

Acknowledgements Dr. Amit Kumar Singh thanks Indian Council of Medical Research (ICMR) and Indian National Science Academy (INSA), New Delhi, India. Gizachew Muluneh Amera thanks the College of Natural Science, Wollo University, Dessie, Ethiopia for the sponsorship. The authors also thank Sharda University and Supercomputing Facility for Bioinformatics & Computational Biology, IIT Delhi.

Compliance with ethical standards

Conflict of interest The authors declare that they have no conflict of interest.

Ethical standards Ethical standards are compulsory for studies relating to human and animal subjects.

References

- Howard A, O'Donoghue M, Feeney A, Sleator RD (2012) *Acinetobacter baumannii*: an emerging opportunistic pathogen. *Virulence* 3:243–250
- Chaari A, Mnif B, Bahloul M, Mahjoubi F, Chtara K, Turki O et al (2013) *Acinetobacter baumannii* ventilator-associated pneumonia: epidemiology, clinical characteristics, and prognosis factors. *Int J Infect Dis* 17:e1225–e12e8
- Jiménez-Guerra G, Heras-Cañas V, Gutiérrez-Soto M, del Pilar Aznarte-Padial M, Expósito-Ruiz M, Navarro-Marí JM et al (2018) Urinary tract infection by *Acinetobacter baumannii* and *Pseudomonas aeruginosa*: evolution of antimicrobial resistance and therapeutic alternatives 67:790–797
- Ni S, Li S, Yang N, Zhang S, Hu D, Li Q et al (2015) Post-neurosurgical meningitis caused by *acinetobacter baumannii*: case series and review of the literature. *Int J Clin Exp Med* 8:21833–21838
- Al-Anazi KA, Abdalhamid B, Alshibani Z, Awad K, Alzayed A, Hassan H et al (2012) *Acinetobacter baumannii* septicemia in a recipient of an allogeneic hematopoietic stem cell transplantation. *Case Rep Transplant* 2012:646195
- Santajit S, Indrawattana N (2016) Mechanisms of antimicrobial resistance in ESKAPE pathogens. *Biomed Res Int* 2016:2475067
- Dijkshoorn L, Nemec A, Seifert H (2007) An increasing threat in hospitals: multidrug-resistant *Acinetobacter baumannii*. *Nat Rev Microbiol* 5:939–951
- Singh H, Thangaraj P, Chakrabarti A (2013) *Acinetobacter baumannii*: a brief account of mechanisms of multidrug resistance and current and future therapeutic management. *J Clin Diagn Res* 7: 2602–2605
- Shrivastava S, Shrivastava P, Ramasamy J (2018) Utilizing a toolkit to respond to the health needs of migrant people in the European region: World Health Organization 9:44–45
- Nelson RE, Schweizer ML, Perencevich EN, Nelson SD, Khader K, Chiang H-Y et al (2016) Costs and mortality associated with multidrug-resistant healthcare-associated *Acinetobacter* infections. *Infect Control Hosp Epidemiol* 37:1212–1218
- Teerawattanapong N, Panich P, Kulpokin D, Na Ranong S, Kongpakwattana K, Saksinanon A et al (2018) A systematic review of the burden of multidrug-resistant healthcare-associated infections among intensive care unit patients in Southeast Asia: the rise of multidrug-resistant *Acinetobacter baumannii*. *Infect Control Hosp Epidemiol* 39:525–533
- Bugg TDH, Braddick D, Dowson CG, Roper DI (2011) Bacterial cell wall assembly: still an attractive antibacterial target. *Trends Biotechnol* 29:167–173

13. Kim HU, Kim TY, Lee SY (2010) Genome-scale metabolic network analysis and drug targeting of multi-drug resistant pathogen *Acinetobacter baumannii* AYE. *Mol BioSyst* 6:339–348
14. Bugg TDH, Walsh CT (1992) Intracellular steps of bacterial cell wall peptidoglycan biosynthesis: enzymology, antibiotics, and antibiotic resistance. *Nat Prod Rep* 9:199–215
15. Meroueh SO, Bencze KZ, Heseck D, Lee M, Fisher JF, Stemmler TL et al (2006) Three-dimensional structure of the bacterial cell wall peptidoglycan 103:4404–4409
16. Barreteau H, Kovač A, Boniface A, Sova M, Gobec S, Blanot D (2008) Cytoplasmic steps of peptidoglycan biosynthesis. *FEMS Microbiol Rev* 32:168–207
17. Chattaway FW *Microbial cell walls and membranes: by H J Rogers, H R Perkins and J B Ward*. pp 564. Chapman & Hall, London. 1980 £30. ISBN 0-412-12030-5. 1982, 10, 33
18. Heijenoort JV Chapter 3 Biosynthesis of the bacterial peptidoglycan unit. In: *New comprehensive biochemistry*, Ghuysen, J.M., Hakenbeck, R. Eds., Elsevier, 1994, Vol. 27, pp. 39–54
19. Bertrand JA, Auger G, Fanchon E, Martin L, Blanot D, van Heijenoort J et al (1997) Crystal structure of UDP-N-acetylmuramoyl-L-alanine: D-glutamate ligase from *Escherichia coli* 16:3416–3425
20. Berman HM, Westbrook J, Feng Z, Gilliland G, Bhat TN, Weissig H et al (2000) The protein data bank. *Nucleic Acids Res* 28:235–242
21. Bertrand JA, Auger G, Martin L, Fanchon E, Blanot D, Le Beller D et al (1999) Determination of the MurD mechanism through crystallographic analysis of enzyme complexes. *J Mol Biol* 289:579–590
22. Kaur N, Khokhar M, Jain V, Bharatam PV, Sandhir R, Tewari R (2013) Identification of druggable targets for *Acinetobacter baumannii* via subtractive genomics and plausible inhibitors for MurA and MurB. *Appl Biochem Biotechnol* 171:417–436
23. Ahmad S, Murtaza UA, Raza S, Azam SS (2019) Blocking the catalytic mechanism of MurC ligase enzyme from *Acinetobacter baumannii*: an in silico guided study towards the discovery of natural antibiotics. *J Mol Liq* 281:117–133
24. Amara GM, Khan RJ, Pathak A, Kumar A, Singh AK (2019) Structure based in-silico study on UDP-N-acetylmuramoyl-L-alanyl-D-glutamate-2,6-diaminopimelate ligase (MurE) from *Acinetobacter baumannii* as a drug target against nosocomial infections. *Inform Med Unlocked* 16:100216
25. Ahmad S, Raza S, Uddin R, Azam SS (2017) Binding mode analysis, dynamic simulation and binding free energy calculations of the MurF ligase from *Acinetobacter baumannii*. *J Mol Graph Model* 77:72–85
26. Amara GM, Khan RJ, Pathak A, Jha RK, Muthukumar J, Singh AK (2019) Screening of promising molecules against MurG as drug target in multi-drug-resistant-*Acinetobacter baumannii* - insights from comparative protein modeling, molecular docking and molecular dynamics simulation. *J Biomol Struct Dyn*:1–23
27. Consortium TU (2018) UniProt: a worldwide hub of protein knowledge. *Nucleic Acids Res* 47:D506–DD15
28. Gasteiger E, Hoogland C, Gattiker A, Duvaud Se, Wilkins MR, Appel RD et al (2005) Protein Identification and Analysis tools on the ExPASy server. In: *The proteomics protocols handbook*, Walker, J.M. Ed., Humana Press, Totowa, pp. 571–607
29. Yu NY, Wagner JR, Laird MR, Melli G, Rey S, Lo R et al (2010) PSORTb 3.0: improved protein subcellular localization prediction with refined localization subcategories and predictive capabilities for all prokaryotes. *Bioinformatics* 26:1608–1615
30. Deng W, Wang C, Zhang Y, Xu Y, Zhang S, Liu Z et al (2016) GPS-PAIL: prediction of lysine acetyltransferase-specific modification sites from protein sequences. *Sci Rep* 6:39787
31. Chauhan JS, Bhat AH, Raghava GPS, Rao A (2012) GlycoPP: a webserver for prediction of N- and O-glycosites in prokaryotic protein sequences. *PLoS One* 7:e40155
32. Pan Z, Wang B, Zhang Y, Wang Y, Ullah S, Jian R et al (2015) dbPSP: a curated database for protein phosphorylation sites in prokaryotes. *Database (Oxford)* 2015:bav031–bav
33. Gupta A, Deshpande A, Amburi JK, Sabarinathan R, Senthilkumar R, Sekar K (2009) CSSP (Consensus Secondary Structure Prediction): a web-based server for structural biologists 42:336–338
34. King RD, Sternberg MJ (1996) Identification and application of the concepts important for accurate and reliable protein secondary structure prediction. *Protein Sci* 5:2298–2310
35. Guermeur Y, Geourjon C, Gallinari P, Deleage G (1999) Improved performance in protein secondary structure prediction by inhomogeneous score combination. *Bioinformatics (Oxford, England)* 15: 413–421
36. Jones DT (1999) Protein secondary structure prediction based on position-specific scoring matrices. *J Mol Biol* 292:195–202
37. Rost B, Sander C (1993) Secondary structure prediction of all-helical proteins in two states. *Protein Eng* 6:831–836
38. Rice P, Longden I, Bleasby A (2000) EMBOSS: the European molecular biology open software suite. *Trends Genet* 16:276–277
39. Pieper U, Eswar N, Webb BM, Eramian D, Kelly L, Barkan DT et al (2008) Modbase, a database of annotated comparative protein structure models and associated resources. *Nucleic Acids Res* 37: D347–DD54
40. DeLano WF (2002) The PyMOL molecular graphics system. DeLano Scientific
41. Biovia DS (2019) Discovery studio visualization Dassault Systèmes BIOVIA
42. Krieger E, Joo K, Lee J, Raman S, Thompson J et al (2009) Improving physical realism, stereochemistry, and side-chain accuracy in homology modeling: four approaches that performed well in CASP8 77:114–122
43. Laskowski RA, MacArthur MW, Moss DS, Thornton JM (1993) PROCHECK: a program to check the stereochemical quality of protein structures 26:283–291
44. Colovos C, Yeates TO (1993) Verification of protein structures: patterns of nonbonded atomic interactions 2:1511–1519
45. Eisenberg D, Lüthy R, Bowie JU (1997) [20] VERIFY3D: assessment of protein models with three-dimensional profiles. *Methods in enzymology*, vol 277. Academic Press, pp 396–404
46. Ye Y, Godzik A (2003) Flexible structure alignment by chaining aligned fragment pairs allowing twists. *Bioinformatics (Oxford, England)* 19(Suppl 2):ii246–ii255
47. Irwin JJ, Shoichet BK (2005) ZINC – a free database of commercially available compounds for virtual screening. *J Chem Inf Model* 45:177–182
48. Viswanathan U, Tomlinson SM, Fonner JM, Mock SA, Watowich SJ (2014) Identification of a novel inhibitor of dengue virus protease through use of a virtual screening drug discovery web portal. *J Chem Inf Model* 54:2816–2825
49. Trott O, Olson AJ (2010) AutoDock Vina: Improving the speed and accuracy of docking with a new scoring function, efficient optimization, and multithreading 31:455–461
50. Nguyen PTV, Yu H, Keller PA (2018) Molecular docking studies to explore potential binding pockets and inhibitors for Chikungunya virus envelope glycoproteins. *Interdiscip Sci* 10:515–524
51. Hetényi C, van der Spoel D (2006) Blind docking of drug-sized compounds to proteins with up to a thousand residues 580:1447–1450
52. Ghersi D, Sanchez R (2009) Improving accuracy and efficiency of blind protein-ligand docking by focusing on predicted binding sites 74:417–424

53. Sander T, Freyss J, von Korff M, Rufener C (2015) DataWarrior: an open-source program for chemistry aware data visualization and analysis. *J Chem Inf Model* 55:460–473
54. Lipinski CA (2004) Lead- and drug-like compounds: the rule-of-five revolution. *Drug Discov Today Technol* 1:337–341
55. Daina A, Michielin O, Zoete V (2017) SwissADME: a free web tool to evaluate pharmacokinetics, drug-likeness and medicinal chemistry friendliness of small molecules. *Sci Rep* 7:42717
56. Alonso H, Bliznyuk AA, Gready JE (2006) Combining docking and molecular dynamic simulations in drug design 26:531–568
57. Van Der Spoel D, Lindahl E, Hess B, Groenhof G, Mark AE, Berendsen HJC (2005) GROMACS: fast, flexible, and free. 26, 1701–18
58. Pol-Fachin L, Fernandes CL, Verli H (2009) GROMOS96 43a1 performance on the characterization of glycoprotein conformational ensembles through molecular dynamics simulations. *Carbohydr Res* 344:491–500
59. Schuttelkopf AW, van Aalten DMF (2004) PRODRG: a tool for high-throughput crystallography of protein-ligand complexes. *Acta Crystallogr Sect D* 60:1355–1363
60. Khan RJ, Jha RK, Amera GM, Jain M, Singh E, Pathak A et al (2020) Targeting SARS-CoV-2: a systematic drug repurposing approach to identify promising inhibitors against 3C-like proteinase and 2'-O-ribose methyltransferase. *J Biomol Struct Dyn*:1–14
61. Mark P, Nilsson L (2001) Structure and dynamics of the TIP3P, SPC, and SPC/E water models at 298 K. *J Phys Chem A* 105:9954–9960
62. Hess B, Bekker H, Berendsen HJC, Fraaije JGEM (1997) LINCS: a linear constraint solver for molecular simulations 18:1463–1472
63. Parrinello M, Rahman A (1981) Polymorphic transitions in single crystals: a new molecular dynamics method 52:7182–7190
64. Darden T, York D, Pedersen L (1993) Particle mesh Ewald: An N-log(N) method for Ewald sums in large systems 98:10089–10092
65. Genheden S, Ryde U (2015) The MM/PBSA and MM/GBSA methods to estimate ligand-binding affinities. *Expert Opin Drug Discovery* 10:449–461
66. Xue J, Huang X, Zhu Y (2019) Using molecular dynamics simulations to evaluate active designs of cephradine hydrolase by molecular mechanics/Poisson–Boltzmann surface area and molecular mechanics/generalized born surface area methods. *RSC Adv* 9: 13868–13877
67. Homeyer N, Gohlke H (2012) Free energy calculations by the molecular mechanics Poisson–Boltzmann surface area method. *Mol Inform* 31:114–122
68. Kumari R, Kumar R, Lynn A (2014) g_mmpbsa—a GROMACS tool for high-throughput MM-PBSA calculations. *J Chem Inf Model* 54:1951–1962
69. Tiwari V (2019) Post-translational modification of ESKAPE pathogens as a potential target in drug discovery. *Drug Discov Today* 24:814–822
70. Micheletti C (2013) Comparing proteins by their internal dynamics: exploring structure–function relationships beyond static structural alignments. *Phys Life Rev* 10:1–26
71. Anderson AC (2003) The process of structure-based drug design. *Chem Biol* 10:787–797
72. Laskowski RA, Jabłońska J, Pravda L, Vařeková RS, Thornton JM (2018) PDBsum: structural summaries of PDB entries 27:129–134
73. Cheng T, Li Q, Zhou Z, Wang Y, Bryant SH (2012) Structure-based virtual screening for drug discovery: a problem-centric review. *AAPS J* 14:133–141
74. Morris GM, Lim-Wilby M (2008) Molecular docking. In: Kukol A (ed) *Molecular modeling of proteins*. Humana Press, Totowa, pp 365–382
75. Kitchen DB, Decornez H, Furr JR, Bajorath J (2004) Docking and scoring in virtual screening for drug discovery: methods and applications. *Nat Rev Drug Discov* 3:935–949
76. Amera GM, Khan RJ, Pathak A, Jha RK, Muthukumaran J, Singh AK (2020) Computer aided ligand based screening for identification of promising molecules against enzymes involved in peptidoglycan biosynthetic pathway from *Acinetobacter baumannii*. *Microb Pathog*:104205
77. Scott P, Deye G, Srinivasan A, Murray C, Moran K, Hulten E et al (2007) An outbreak of multidrug-resistant *Acinetobacter baumannii*-calcoaceticus complex infection in the US military health care system associated with military operations in Iraq. *Clin Infect Dis* 44:1577–1584
78. Shelburne SA, Singh KV, White AC, Byrne L, Carmer A, Austin C et al (2008) Sequential outbreaks of infections by distinct *Acinetobacter baumannii* strains in a public teaching hospital in Houston, Texas 46:198–205
79. Hujer AM, Higgins PG, Rudin SD, Buser GL, Marshall SH, Xanthopoulos K et al (2017) Nosocomial outbreak of extensively drug-resistant *Acinetobacter baumannii* isolates containing blaOXA-237 carried on a plasmid 61:e00797–e00717
80. Zhao Y, Hu K, Zhang J, Guo Y, Fan X, Wang Y et al (2019) Outbreak of carbapenem-resistant *Acinetobacter baumannii* carrying the carbapenemase OXA-23 in ICU of the eastern Heilongjiang Province, China. *BMC Infect Dis* 19:452
81. Gimeno A, Ojeda-Montes MJ, Tomás-Hernández S, Cereto-Massagué A, Beltrán-Debón R, Mulero M et al (2019) The light and dark sides of virtual screening: what is there to know? 20:1375
82. Marklund EG, Benesch JL (2019) Weighing-up protein dynamics: the combination of native mass spectrometry and molecular dynamics simulations. *Curr Opin Struct Biol* 54:50–58

Publisher's note Springer Nature remains neutral with regard to jurisdictional claims in published maps and institutional affiliations.